

# Mirroring and Nonlinear Perturbation of a Circuit's System with Multiple Attractors

Emile Franc Doungmo Goufo

*Department of Mathematical Sciences, University of South Africa*  
0003 Florida, South Africa  
E-mail(*corresp.*): [franckemile2006@yahoo.ca](mailto:franckemile2006@yahoo.ca)

Received February 21, 2024; accepted July 8, 2024

**Abstract.** We infix the duality-symmetric and the mirror symmetry conversion processes into a dynamical system representing an electric circuit diagram with three input (or output) as shown in Figure 2. Hence, a new non-linear variable order initial value problem is obtained and solved using the Haar wavelet numerical method (HWNM). Error, stability and entropy analyzes show the reliability of the method. Numerical simulations are then implemented and show for the new system, existence of various attractors' types (point attractors (PAs), limit cycles, strange attractors (SAs), double attractor (DA), coexisting attractors (CoAs)) with their mirror reflections. Both are in a symmetrical structure in which they face each other, separated by a changing symmetry line and exhibiting similar properties. The circuit implementation using a Field Programmable Gate Array (FPGA) is performed and concur with the expected results.

**Keywords:** electric circuit diagram, limit cycles, mirror symmetry conversion process, perturbation, circuit implementation.

**AMS Subject Classification:** 34A34; 37Fxx; 37D45; 26A33; 34D10; 47N70.

## 1 Introduction

### 1.1 Mirroring remarks

In everyday life, the mirror process is sometimes opposed or compared to the matching art (as one can see in Figure 1 (left)). It occurs in areas like social science, psychology, psychobiology, neuropsychology, cognitive science, economics, anthropology and many other behavioral sciences [8, 21]. The principal objective is to impact the behavior of humans and/or animals through naturalistic

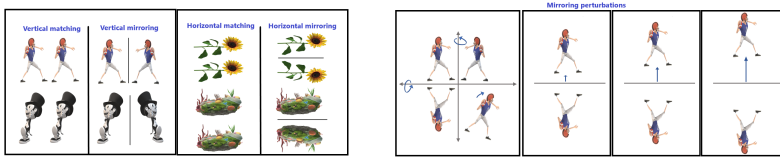


**Figure 1.** (Left) Mirroring vs matching in real life. (Right) Mirroring perturbations and transformations.

observation. It may enhance, for instance, communication effectiveness in sales presentations, objection handling and customer service.

In a mathematical point of view, both mirror and matching processes can apply the method of images which consists of extending the domain of the solution to a differential equation by adding another domain. This is especially the case for mirror process where the additional domain is obtained via the solution’s mirror image with respect to a symmetry (hyper)plane. The resulting mirror system can therefore be perturbed via mathematical operations such as rotation, translation, etc., as shown in Figure 1 (right).

This leads to an intriguing question: Is it also possible to get a similar perturbation results using the model’s parameters? We try to bring an answer by solving a system of differential equations and analysing its related electronic circuit model.

### 1.2 Preliminaries

Chaos and bifurcating behavior became subject of interest for the scientific community more than five decades ago when Lorenz developed and described his well known attractor [4,10,15]. Doors were then open, marking the starting point of a series of researches which led to a panoply of new types of chaotic perturbations. Number of scientific fields related to such dynamics, including synchronization or chaos control and application were also developed and are better understood today. Innovative ideas have also been introduced paving the way for a better understanding of the concepts underlying chaos phenomenon. A variety of techniques capable of producing chaotic behaviors were proposed along side with techniques able to control or synchronize some of them [11,14,16]. The authors in [5] for instance, investigated the dynamical trajectories of a chaotic oscillator of order three which is non-linear and whose non-linear element contains a threshold controller. They managed to show existence of a certain number of complex dynamics together with the coexistence of multiple attractors. The impacts of metaheuristic and swarm intelligence approach in optimization have also been studied [2].

DEFINITION 1 [Time-variable order operator [3,9]]. Consider  $\epsilon : \mathbb{R}_+ \ni \theta \mapsto [0, 1]$ , to be a continuous function, consider  $h : \mathbb{R}_+ \ni t \mapsto \mathbb{R}$  to be a continuous and differentiable function, and  $H > 0$ . The variable order derivative of  $h$  in

$[0, H)$  is defined as:

$$D_t^{\epsilon(\theta)} h(t) = \frac{1}{\Gamma(1 - \epsilon(\theta))} \int_0^t (t - \epsilon)^{-\epsilon(\theta)} h'(\epsilon) d\epsilon, \text{ with } t \in [0, H), \theta \in \mathbb{R}_+. \quad (1.1)$$

This operator exhibits the advantage that its derivative of a constant vanishes. Its associated integral operator with variable order  $\epsilon(\theta)$  reads as

$$I_t^{\epsilon(\theta)} h(t) = \int_0^t \frac{1}{\Gamma(\gamma(t))} (t - \epsilon)^{\epsilon(\theta)-1} h(\epsilon) d\epsilon, \text{ with } t \in [0, H), \theta \in \mathbb{R}_+. \quad (1.2)$$

### 1.3 Description of the electric circuit diagram

In this section, we are interested in the electric circuit diagram depicted in Figure 2,

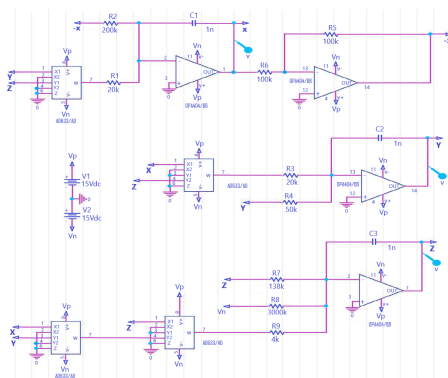


**Figure 2.** The circuit diagram used in the circuit realization of system (1.3).

which can be used for the circuit realization of the following system

$$\begin{cases} D_t^{\epsilon(\theta)} \mathbf{x}(t) = \gamma_1 \mathbf{x} - 2\mathbf{y}\mathbf{z}, \\ D_t^{\epsilon(\theta)} \mathbf{y}(t) = -\gamma_2 \mathbf{y} + 2\mathbf{x}\mathbf{z}, \\ D_t^{\epsilon(\theta)} \mathbf{z}(t) = -\gamma_3 \mathbf{z} + \mathbf{x}\mathbf{y}\mathbf{z} + \frac{1}{2}r. \end{cases} \quad (1.3)$$

Note that this system is restricted from saturation of circuit elements, which was done by reducing the voltage values of the circuit. Hence we have to first consider a more global system with no restriction. Such a model can be obtained from the system (1.3) using variables scaling by setting:  $\mathbf{x} = x$ ,  $\mathbf{y} = y$  and  $\mathbf{z} = \frac{1}{2}z$ . This transformation yields the system

$$\begin{cases} D_t^{\epsilon(\theta)} x(t) = \gamma_1 x - yz, \\ D_t^{\epsilon(\theta)} y(t) = -\gamma_2 y + xz, \\ D_t^{\epsilon(\theta)} z(t) = -\gamma_3 z + xyz + r, \end{cases} \quad (1.4)$$

where  $x, y, z$  are real state variables and  $\gamma_1, \gamma_2, \gamma_3$  and  $r$  are constant real parameters. To this model, we can associate the following initial conditions for the sake of solvability.

$$x(0) = \hat{x}(x), \quad y(0) = \hat{y}(y), \quad z(0) = \hat{z}(z). \tag{1.5}$$

## 2 Attractors' evolution in the case $\epsilon(\theta) = 1$

When  $\epsilon(\theta) = 1$ , the model (1.4) becomes

$$\begin{cases} D_t^1 x(t) = \frac{dx(t)}{dt} = \gamma_1 x - yz, \\ D_t^1 y(t) = \frac{dy(t)}{dt} = -\gamma_2 y + xz, \\ D_t^1 z(t) = \frac{dz(t)}{dt} = -\gamma_3 z + xyz + r. \end{cases} \tag{2.1}$$

The standard graphical simulation of system (2.1) shows that it is characterized by an attractor of type butterfly as depicted by Figure 3 for the parameter values  $\gamma_1 = 4, \gamma_2 = 9, \gamma_3 = 4, r = 4$  and initial conditions  $\check{x} = 1, \check{y} = 1$  and  $\check{z} = 1$ . In Figure 4, are depicted two times series of variable  $z$ , formed for 2 different initial conditions, which are (a) ( $\check{x} = 1, \check{y} = 1$  and  $\check{z} = 1$ ) and ( $\check{x} = 1, \check{y} = 1$  and  $\check{z} = 1.001$ ), respectively.

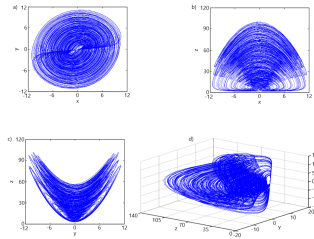


**Figure 3.** Two and three dimensional attractor of type butterfly characterizing the system (2.1), for the parameter values  $\gamma_1 = 4, \gamma_2 = 9, \gamma_3 = 4, r = 4$  and initial conditions  $\check{x} = 1, \check{y} = 1$  and  $\check{z} = 1$ .

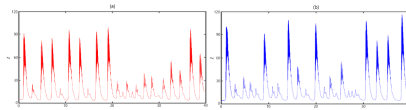


**Figure 4.** Times series of variable  $z$  for the initial conditions: (a)  $\check{x} = 1, \check{y} = 1$  and  $\check{z} = 1$ . (b)  $\check{x} = 1, \check{y} = 1$  and  $\check{z} = 1.001$ .

The disparities between these two figures show how sensitive is the dependence of the model (2.1) on its initial conditions, while making the subsequent trajectories of the system non predictable in a longer range of time ( $t \gg \gg 0$ .) Using the crossing section given by  $\Pi = \{(y, z) \in \mathbb{R}^2 : x = 0\}$ , we can depict the Poincaré map of the model (2.1) as presented in Figure 5(a) and which proves that the Poincaré map in this system is a collection of points. The

Lyapunov exponents of the system (2.1) for  $\gamma_3 \in (0, 6)$  is shown in Figure 5(b) and when fixing the following parameter values as  $\gamma_1 = 2$  and  $r = 4$  we obtain the bifurcating dynamics for the model (2.1) when it varies with respect to the parameter  $\gamma_3$ . The bifurcation diagrams, for a varying  $\gamma_3$  are depicted in Figure 6 for  $\gamma_2 = 0.02, 1.02, 8$  and they show that the dynamical evolutions of the system lead to attractors.

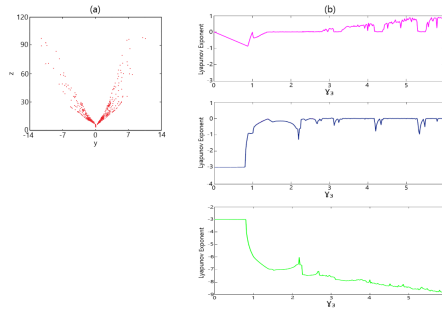


**Figure 5.** (a) Poincaré map of the model (2.1) using the crossing section given by  $\Pi = \{(y, z) \in \mathbb{R}^2 : x = 0\}$ , showing a collection of points. (b) Lyapunov exponents of the system (2.1) for  $\gamma_3 \in (0, 6)$ .

For  $\gamma_2 = 0.02$ , we have the coexistence of only two foci located on the sections  $F_{\pm}$  together with a saddle on  $F_*$ . Therefore, the foci evolve to limit cycles using Hopf bifurcations (HB) as depicted in shown in Figure 6 (a), where limit cycles coexist. A similar scenario is shown in Figure 6 (b) for  $\gamma_2 = 1.02$ . Further increase of  $\gamma_2$  may result in the cascade of period-doubling bifurcation associated with the limit cycles as shown in Figure 6 (c). Different types of coexistence can arise in the system, such as the coexistence of limit cycles and a chaotic attractors (CA). The illustration of some of these attractors can be seen in Figure 7 for two different values of parameter  $\gamma_3$ , namely  $\gamma_3 = 1.2$  in Figure 7 a) and  $\gamma_3 = 1.4$  in Figure 7 b).

### 3 Case of a general variable order $\epsilon(\theta)$ : induction of symmetrical fractal structure

This section is all about setting the model and generating a symmetrical fractal structure. The case where the variable order  $\epsilon(\theta)$  covers its general definition is considered here. Hence, using the perturbation method, we start by introducing into (1.4) two functions: A duality-symmetric function denoted by  $\chi$ , which depends on the variable  $y$  and a function symbolizing the mirror reflecting operation denoted by  $\varpi$ . Such a procedure leads to a new model given as follows:

$$\begin{cases} D_t^{\epsilon(\theta)} x(t) = \gamma_1 x - yz, \\ D_t^{\epsilon(\theta)} y(t) = -\gamma_2 \chi(y) + xz, \\ D_t^{\epsilon(\theta)} z(t) = -\gamma_3 z + x\chi(y)z + r, \end{cases}$$

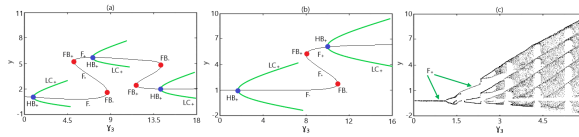


**Figure 6.** The bifurcation diagrams with the typical cases depending on the variation of  $\gamma_3$  for (a)  $\gamma_2 = 0.02$ ; (b)  $\gamma_2 = 1.02$  and (c)  $\gamma_2 = 8$ , all showing the system (2.1) has dynamical evolutions that lead to attractors.

which becomes after inserting  $\varpi$ ,

$$\begin{cases} D_t^{\epsilon(\theta)} x(t) = \gamma_1 x - yz, \\ D_t^{\epsilon(\theta)} y(t) = -\gamma_2 \chi(y) + x \times [\text{sgn}(z - \check{z}) \times (z - \check{z}) - \varpi(z)], \\ D_t^{\epsilon(\theta)} z(t) = -\gamma_3 [(z - \check{z}) + \text{sgn}(z - \check{z}) \times \varpi(z)] \\ \quad + x \times \chi(y) \times [\text{sgn}(z - \check{z}) \times (z - \check{z}) - \varpi(z)] + r. \end{cases} \tag{3.1}$$

In the later system, the duality-symmetric function  $\chi(y)$  represents a multi-segment non-quadratic function and its expression reads as

$$\chi(y) = U_0 y + \sum_{l=1}^m U_l \left( \text{sgn}(y + \check{U}_l) - \text{sgn}(y - \check{U}_l) - 1 \right),$$

here  $l = 1, 2, \dots, m$  and  $\mathbb{N} \ni m \geq 1$ . The family  $U_l, l = 0, 1, 2, \dots, m$  and  $\check{U}_l$  are defined by

$$U_0 = \tau, U_l = \frac{\alpha}{\tau_l}, \check{U}_l = \frac{\alpha}{2\tau}(l + 1).$$

As for the  $\varpi(z)$  function, it characterizes in the system the mirror symmetry

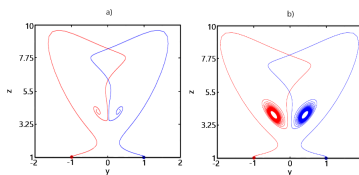


**Figure 7.** Attractors of the system (2.1) for  $\gamma_3 = 1.2$  in a) and  $\gamma_3 = 1.4$  in b).

conversion process and its expression reads as

$$\varpi(z) = \sum_{l=1}^M (\pm\theta \cdot (1 \pm \text{sgn}(\text{sgn}(z - \check{z}) \times (z - \check{z}) - (z_l - \check{z}))))), \tag{3.2}$$

where  $M \geq 1, \check{z}, \tau, \theta, \alpha, z_l, l = 1, 2, \dots, M$  are all real numbers. Now, that we have perturbed and got the system (3.1) with  $\chi(y)$  and  $\varpi(z)$ , it is time to solve it and assess the impact of the said perturbation. Recall that the initial

conditions (1.5) are associated to the system (3.1). Then it is possible to make use of the state vectors in order to put the model (3.1) into a compact form. To do that, we simplify the notations as

$\mathbf{w}(t) = (x(t), y(t), z(t))$ ;  $\mathbf{w}_0(x, y, z) = \mathbf{w}(0) = (x(0), y(0), z(0)) = (\hat{x}, \hat{y}, \hat{z})$ . Moreover, the  $x, y, z$ -dependent matrix  $\mathfrak{J}$  given as

$$\mathfrak{J}(\mathbf{w}(t), t) = \mathfrak{J}(x(t), y(t), z(t), t) = (\mathfrak{J}_1(\mathbf{w}(t), t), \mathfrak{J}_2(\mathbf{w}(t), t), \mathfrak{J}_3(\mathbf{w}(t), t)),$$

leads to the system

$$\begin{cases} \mathfrak{J}_1(\mathbf{w}(t), t) = \mathfrak{J}_1(x(t), y(t), z(t), t) = \gamma_1 x - yz, \\ \mathfrak{J}_2(\mathbf{w}(t), t) = \mathfrak{J}_2(x(t), y(t), z(t), t) = -\gamma_2 \chi(y) \\ \quad + x \times [\text{sgn}(z - \check{z}) \times (z - \check{z}) - \varpi(z)], \\ \mathfrak{J}_3(\mathbf{w}(t), t) = \mathfrak{J}_3(x(t), y(t), z(t), t) = -\gamma_3 [(z - \check{z}) + \text{sgn}(z - \check{z}) \times \varpi(z)] \\ \quad + x \times \chi(y) \times [\text{sgn}(z - \check{z}) \times (z - \check{z}) - \varpi(z)] + r. \end{cases}$$

This system can therefore be reduced to a compact form and referring to the model (3.1) we have the following equation  $D_t^{\epsilon(\theta)} \mathbf{w}(t) = \mathfrak{J}(\mathbf{w}(t), t)$ , equivalently,

$$D_t^{\epsilon(\theta)} x(t) = \mathfrak{J}_1(\mathbf{w}(t), t), \quad D_t^{\epsilon(\theta)} y(t) = \mathfrak{J}_2(\mathbf{w}(t), t), \quad D_t^{\epsilon(\theta)} z(t) = \mathfrak{J}_3(\mathbf{w}(t), t), \quad (3.3)$$

satisfying the initial conditions:  $x(0) = \hat{x}(x)$ ,  $y(0) = \hat{y}(y)$ ,  $z(0) = \hat{z}(z)$ . At this step, we can use a suitable numerical method to address the solvability of the Cauchy problem expressed above. The most adequate method is the HWNM defined in [1], which enables us to find and express the best approximation of the state vector  $\mathbf{w}$ . To achieve it, we make use of a system of basis functions, denoted as  $\mathfrak{B}_{a,b}$  and called the Haar orthonormal basis system.

$$\mathbf{w}(t) \approx \mathbf{w}_\pi(t) = \sum_{a=1}^{\mathbf{m}} \sum_{b=0}^{\pi-1} \mathfrak{B}_{a,b} \mathbf{p}_{a,b}(t), \quad \text{with } \pi \in \{2^e : e = 0, 1, 2, 3, \dots\}, \quad (3.4)$$

$$\mathfrak{B}_{a,b} = \langle \mathbf{w}, \mathbf{p}_{a,b} \rangle = \int_0^\infty \mathbf{w}(t) \mathbf{p}_{a,b}(t) dt.$$

The kernel  $\mathbf{p}_{a,b}$  appearing inside the integral is called the Haar function and its definition is given by

$$\mathbf{p}_{a,b}(t) = \mathbf{p}_b(t - a + 1), \quad a = 1, 2, \dots, \mathbf{m} \quad \text{and} \quad b = 0, 1, 2, 3, \dots, \quad (3.5)$$

where

$$\mathbf{p}_b(t) = \begin{cases} 2^{\frac{b}{2}} F_h(2^i t - \pi), & \text{for } b = 1, 2, \dots; \\ 1, & \text{for } b = 0, \end{cases} \quad (3.6)$$

and

$$F_h(t) = \begin{cases} 1, & \text{if } t \in [0, 1/2[; \\ -1, & \text{if } t \in [1/2, 1[; \\ 0, & \text{everywhere else.} \end{cases}$$

To get these results, we have made use of the power property for discrete numbers that can be summarized as follows: considering any number  $b \in \{0, 1, 2, 3, \dots\}$ , it can always be written into the sum with power  $b = 2^e + \pi$  with  $e = 0, 1, 2, 3, \dots$  and  $\pi = 0, 1, 2, 3, \dots, 2^e - 1$ . Recall that the approximation scheme expressed in (3.4) can also take an explicit matrix form and becomes

$$\mathbf{w}(t) \approx \mathbf{w}_\pi(t) = \mathbf{g}_{\mathbf{m}\pi \times 1}^T \mathbf{q}_{\mathbf{m}\pi \times 1},$$

where the vector  $\mathbf{g}_{\mathbf{m}\pi \times 1}$  is defined by

$$\mathbf{g}_{\mathbf{m}\pi \times 1} = (\mathfrak{B}_{1,0}, \dots, \mathfrak{B}_{1,\pi-1}, \mathfrak{B}_{2,0}, \dots, \mathfrak{B}_{2,\pi-1}, \dots, \mathfrak{B}_{\mathbf{m},0}, \dots, \mathfrak{B}_{\mathbf{m},\pi-1},)$$

and the transpose  $^T \mathbf{q}_{\mathbf{m}\pi \times 1}$  of the vector  $\mathbf{q}_{\mathbf{m}\pi \times 1}$  reading as

$$\mathbf{q}_{\mathbf{m}\pi \times 1} = (\mathbf{p}_{1,0}, \dots, \mathbf{p}_{1,\pi-1}, \mathbf{p}_{2,0}, \dots, \mathbf{p}_{2,\pi-1}, \dots, \mathbf{p}_{\mathbf{m},0}, \dots, \mathbf{p}_{\mathbf{m},\pi-1},)$$

At this step, we make use of the  $\epsilon(\theta)$ -variable order operator  $D_t^{\epsilon(\theta)}$  defined in (1.1) and where  $\epsilon$  is assumed to vary with respect to the time  $t$ . The application of operator  $D_t^{\epsilon(\theta)}$  yielded the associated system (3.3) and using the analysis performed above leads to the following approximation system

$$\begin{aligned} D_t^{\epsilon(\theta)} x(t) &= \mathfrak{J}_1(\mathbf{w}(t), t) \approx D_t^{\epsilon(\theta)} x_\pi(t) = {}^T \mathbf{g}_{\mathbf{m}\pi \times 1}^1 \mathbf{q}_{\mathbf{m}\pi \times 1}; \\ D_t^{\epsilon(\theta)} y(t) &= \mathfrak{J}_2(\mathbf{w}(t), t) \approx D_t^{\epsilon(\theta)} y_\pi(t) = {}^T \mathbf{g}_{\mathbf{m}\pi \times 1}^2 \mathbf{q}_{\mathbf{m}\pi \times 1}; \\ D_t^{\epsilon(\theta)} z(t) &= \mathfrak{J}_3(\mathbf{w}(t), t) \approx D_t^{\epsilon(\theta)} z_\pi(t) = {}^T \mathbf{g}_{\mathbf{m}\pi \times 1}^3 \mathbf{q}_{\mathbf{m}\pi \times 1}. \end{aligned} \tag{3.7}$$

On both sides of the system (3.7), we apply the inverse operator defined in (1.2) and get

$$\begin{aligned} x(t) &\approx x_\pi(t) = {}^T \mathbf{g}_{\mathbf{m}\pi \times 1}^1 \phi_{\mathbf{m}\pi \times \mathbf{m}\pi}^q \mathbf{q}_{\mathbf{m}\pi \times 1} + \hat{x}; \\ y(t) &\approx y_\pi(t) = {}^T \mathbf{g}_{\mathbf{m}\pi \times 1}^2 \phi_{\mathbf{m}\pi \times \mathbf{m}\pi}^q \mathbf{q}_{\mathbf{m}\pi \times 1} + \hat{y}; \\ z(t) &\approx z_\pi(t) = {}^T \mathbf{g}_{\mathbf{m}\pi \times 1}^3 \phi_{\mathbf{m}\pi \times \mathbf{m}\pi}^q \mathbf{q}_{\mathbf{m}\pi \times 1} + \hat{z}. \end{aligned} \tag{3.8}$$

Such a scheme is consistent with our desired result as it includes the operational matrix  $\phi_{\mathbf{m}\pi \times \mathbf{m}\pi}^q$  also called the Haar variable order operational matrix (see equivalent operational matrix in [1]). At this step, the Cauchy problem (3.1)–(1.5) is almost numerically solved if we recall and consider the technique of collocation points via the Galerkin’s method. This leads the existence of residual errors related to the scheme’s use and whose expressions are obtained after substituting both Equations (3.7) and (3.8) into the system (3.1). They are therefore given by

$$\begin{aligned} \mathfrak{f}_1(\mathbf{e}^1, \mathbf{e}^2, \mathbf{e}^3, t) &= {}^T \mathbf{g}_{\mathbf{m}\pi \times 1}^1 \mathbf{q}_{\mathbf{m}\pi \times 1} - \mathfrak{J}_1({}^T \mathbf{g}_{\mathbf{m}\pi \times 1}^1 \phi_{\mathbf{m}\pi \times \mathbf{m}\pi}^q \mathbf{q}_{\mathbf{m}\pi \times 1}, \\ &\quad {}^T \mathbf{g}_{\mathbf{m}\pi \times 1}^2 \phi_{\mathbf{m}\pi \times \mathbf{m}\pi}^q \mathbf{q}_{\mathbf{m}\pi \times 1}, {}^T \mathbf{g}_{\mathbf{m}\pi \times 1}^3 \phi_{\mathbf{m}\pi \times \mathbf{m}\pi}^q \mathbf{q}_{\mathbf{m}\pi \times 1}, t); \\ \mathfrak{f}_2(\mathbf{e}^1, \mathbf{e}^2, \mathbf{e}^3, t) &= {}^T \mathbf{g}_{\mathbf{m}\pi \times 1}^2 \mathbf{q}_{\mathbf{m}\pi \times 1} - \mathfrak{J}_2({}^T \mathbf{g}_{\mathbf{m}\pi \times 1}^1 \phi_{\mathbf{m}\pi \times \mathbf{m}\pi}^q \mathbf{q}_{\mathbf{m}\pi \times 1}, \\ &\quad {}^T \mathbf{g}_{\mathbf{m}\pi \times 1}^2 \phi_{\mathbf{m}\pi \times \mathbf{m}\pi}^q \mathbf{q}_{\mathbf{m}\pi \times 1}, {}^T \mathbf{g}_{\mathbf{m}\pi \times 1}^3 \phi_{\mathbf{m}\pi \times \mathbf{m}\pi}^q \mathbf{q}_{\mathbf{m}\pi \times 1}, t); \\ \mathfrak{f}_3(\mathbf{e}^1, \mathbf{e}^2, \mathbf{e}^3, t) &= {}^T \mathbf{g}_{\mathbf{m}\pi \times 1}^3 \mathbf{q}_{\mathbf{m}\pi \times 1} - \mathfrak{J}_3({}^T \mathbf{g}_{\mathbf{m}\pi \times 1}^1 \phi_{\mathbf{m}\pi \times \mathbf{m}\pi}^q \mathbf{q}_{\mathbf{m}\pi \times 1}, \\ &\quad {}^T \mathbf{g}_{\mathbf{m}\pi \times 1}^2 \phi_{\mathbf{m}\pi \times \mathbf{m}\pi}^q \mathbf{q}_{\mathbf{m}\pi \times 1}, {}^T \mathbf{g}_{\mathbf{m}\pi \times 1}^3 \phi_{\mathbf{m}\pi \times \mathbf{m}\pi}^q \mathbf{q}_{\mathbf{m}\pi \times 1}, t), \end{aligned}$$

where

$$\begin{aligned} \mathbf{e}^1 &= \mathfrak{B}_{1,0}^1, \dots, \mathfrak{B}_{1,\pi-1}^1, \dots, \mathfrak{B}_{\mathbf{m},0}^1, \dots, \mathfrak{B}_{\mathbf{m},\pi-1}^1; \\ \mathbf{e}^2 &= \mathfrak{B}_{1,0}^2, \dots, \mathfrak{B}_{1,\pi-1}^2, \dots, \mathfrak{B}_{\mathbf{m},0}^2, \dots, \mathfrak{B}_{\mathbf{m},\pi-1}^2; \\ \mathbf{e}^3 &= \mathfrak{B}_{1,0}^3, \dots, \mathfrak{B}_{1,\pi-1}^3, \dots, \mathfrak{B}_{\mathbf{m},0}^3, \dots, \mathfrak{B}_{\mathbf{m},\pi-1}^3; \end{aligned}$$

and the components  $\mathfrak{B}_{\cdot, \cdot}^b$  are those of the matrix  ${}^T\mathbf{C}_{\times \cdot}^b$ . With the assumption that

$$f_1(\mathbf{e}^1, \mathbf{e}^2, \mathbf{e}^3, t_{l,b}) = 0; f_2(\mathbf{e}^1, \mathbf{e}^2, \mathbf{e}^3, t_{l,b}) = 0; f_3(\mathbf{e}^1, \mathbf{e}^2, \mathbf{e}^3, t_{l,b}) = 0,$$

it is ultimately easy to get a system of  $3\mathbf{m}\pi$  differential equations containing  $3\mathbf{m}\pi$  unknowns, all represented by

$$\begin{aligned} &\mathfrak{B}_{1,0}^1, \dots, \mathfrak{B}_{1,\pi-1}^1, \dots, \mathfrak{B}_{\mathbf{m},0}^1, \dots, \mathfrak{B}_{\mathbf{m},\pi-1}^1; \\ &\mathfrak{B}_{1,0}^2, \dots, \mathfrak{B}_{1,\pi-1}^2, \dots, \mathfrak{B}_{\mathbf{m},0}^2, \dots, \mathfrak{B}_{\mathbf{m},\pi-1}^2; \\ &\mathfrak{B}_{1,0}^3, \dots, \mathfrak{B}_{1,\pi-1}^3, \dots, \mathfrak{B}_{\mathbf{m},0}^3, \dots, \mathfrak{B}_{\mathbf{m},\pi-1}^3. \end{aligned}$$

In this analysis,  $t_{l,b}$  is defined as  $t_{l,b} = \frac{2^\pi e - 1}{2^\pi} + l - b - 1, \quad l = 1, 2, \dots, \mathbf{m}; \quad b = 1, 2, \dots, \pi$  and it gives all the  $\mathbf{m}\pi$  collocation points that are needful to conveniently realize the desired approximation scheme. Hence, at this level the most difficult part is done and we only have to solve the problem for the required unknowns. With the expressions of these unknowns in hand, it is then straightforward to substitute into (3.8) and finally obtain the intended numerical results as  $\mathbf{w}(t) = (x_\pi(t), y_\pi(t), z_\pi(t))$ .

### 4 Stability of the mirror process and comparison

To assess the chaotic properties of a non-linear dynamical system, people sometime determine and analyze its Lyapunov exponent (LE). For instance, given a non-linear map  $\mathfrak{T}(z_j), 0 \leq j \leq n$  with  $n \in \mathbb{N}$ , the LE reads as

$$\mathfrak{L} = \lim_{n \rightarrow \infty} \frac{1}{n} \sum_{j=0}^{n-1} \ln |\mathfrak{T}'(z_j)|$$

and its value greater than 0 indicates that the map  $\mathfrak{T}$  has turned into a chaotic state, with the said value positively proportional to the map's chaotic manifestation. Due to the fact the  $\epsilon(\theta)$  is variable, we need to find an applicable range where the mirror effect is less dependent and less impacted by the chaotic performance of the system. Then, considering (3.8), (1.1) and (3.2), the approximated system (3.8) is put into a compact form

$$\theta \mathfrak{T}^{\epsilon_k}(z_j), \quad 0 \leq j \leq n \text{ with } n \in \mathbb{N}. \tag{4.1}$$

Putting for instance,  $\epsilon$  as the product of  $\theta$  with another number  $p_0$  (real and arbitrary as  $\epsilon(\theta) = p_0\theta$ ), the summary of the system's state is given in Table 1. Compared with different values of  $\theta$ , the system for  $\theta = 1$  and  $\theta = 1.05$  admits stable performance with less impact on the mirror process while conserving a better complex chaotic behavior, as depicted in Figure 8.

**Table 1.** Different states of the system with the green zone representing a more favorable range.

$\theta$	0	0.3	0.5		0.9		1	
$p_0$	0.95	0.55	0.95	0.55	0.95	0.55	0.95	0.55
State	Ins	Ins	Ins	Ins	Ins	Ins	Sta	Sta
$\theta$	1.05		2	2.5		3	...	
$p_0$	0.95	0.55	0.95	0.55	0.95	0.55	0.95	0.55
State	Sta	Sta	Ins	Ins	Ins	Ins	Ins	...

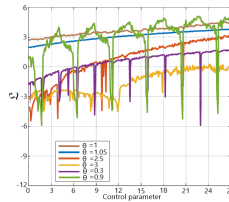


**Figure 8.** Comparison of different performance states of the system.

### 5 System entropy and comparison

In order to measure series complexity based on approximate entropy, we can make use of the sample entropy (SE) by considering again (4.1). For the series  $\{\theta \mathfrak{X}_k^\epsilon(z_1), \theta \mathfrak{X}_k^\epsilon(z_2), \dots, \theta \mathfrak{X}_k^\epsilon(z_V)\}$ ,  $V \in \mathbb{N}$ , and the  $v$ -dimension vector  $\theta \mathfrak{X}_{k+v}^\epsilon(i) = \{\theta \mathfrak{X}_k^\epsilon(z_i), \theta \mathfrak{X}_k^\epsilon(z_{i+1}), \dots, \theta \mathfrak{X}_k^\epsilon(z_{i+v-1})\}$ , the SE is given as [18]  $S = S(v, t_0, V) = \ln \mathcal{D}_v - \ln \mathcal{D}_{v+1}$  where  $\mathcal{D}_v$  indicates the number vectors for which the Chebyshev distance ([20])  $d(\theta \mathfrak{X}_{k+v}^\epsilon(i), \theta \mathfrak{X}_{k+v}^\epsilon(j))$  of the generate vectors is less than the acceptance tolerance number  $t_0$ . Meaning

$$[d(\theta \mathfrak{X}_{k+v}^\epsilon(i), \theta \mathfrak{X}_{k+v}^\epsilon(j)) < t_0].$$

Setting  $v = 2$  and  $t_0 = 0.4$ , the calculations of different SE for the system is depicted in Figure 9. As expected, the results obtained for  $\theta = 1$  and  $\theta = 1.05$  have larger SE values than other cases, which guarantee the mirror aspect with chaotic state for the system with a high complexity. The disparities ( $\Delta \mathfrak{L}$  and  $\Delta S$ ) related to performance and complexity are summarized in Table 2.

### 6 Error tolerance

Any approximation scheme comes with a margin of error and in this section, we are looking for the condition under which the error committed when using the HWNM to solve the problem (3.1)–(1.5) is tolerable. Due to the fact that  $\mathbf{w}$  is from  $L^2[0, \mathbf{m})$  then, we have  $x \in L^2[0, \mathbf{m})$ ,  $y \in L^2[0, \mathbf{m})$  and  $z \in L^2[0, \mathbf{m})$ .

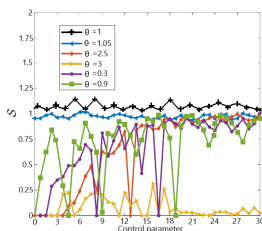


Figure 9. Comparison of different complexity states of the system.

Table 2. Comparison of extreme disparities related to performance and complexity.

	$\theta = 0.3$	$\theta = 0.9$	$\theta = 1$	$\theta = 1.05$	$\theta = 2.5$	$\theta = 3$
Max $\mathcal{L}$	1.5	5.0	4.5	4.0	3.1	0.3
Min $\mathcal{L}$	-6.0	-6.0	2.7	2.0	-5.3	-4.5
$\Delta\mathcal{L}$	7.5	11.0	1.8	2.0	8.4	4.8
Max $\mathcal{S}$	1.000	0.956	1.125	1.011	1.000	0.333
Min $\mathcal{S}$	0	0	1.083	0.916	0	0
$\Delta\mathcal{S}$	1	0.956	0.042	0.095	1	0.333

This allows the equality

$$\|\mathfrak{w}\|_2^2 = \|x\|_{L^2}^2 + \|y\|_{L^2}^2 + \|z\|_{L^2}^2, \tag{6.1}$$

which defines a norm  $\|\mathfrak{w}\|_2$  of  $\mathfrak{w}$  with

$$\|x\|_{L^2}^2 = \int_0^m |x(t)|^2 dt, \quad \|y\|_{L^2}^2 = \int_0^m |y(t)|^2 dt, \quad \|z\|_{L^2}^2 = \int_0^m |z(t)|^2 dt.$$

The consequence drawn from (3.7) to (3.8) is that, the general variable order  $\epsilon(\theta)$ -operator  $D_t^{\epsilon(\theta)} \mathfrak{w}_\pi(t)$  represents an approximation operator for  $D_t^{\epsilon(\theta)} \mathfrak{w}(t)$  as reading in the following expression

$$D_t^{\epsilon(\theta)} \mathfrak{w}_\pi(t) = \sum_{a=1}^m \sum_{b=0}^{\pi-1} \mathfrak{B}_{a,b} \mathbf{P}_{a,b}(t) \left[ \approx D_t^{\epsilon(\theta)} \mathfrak{w}(t) \right].$$

It can be rewritten as

$$\begin{aligned} \left( \begin{array}{c} \sum_{a=1}^m \sum_{b=0}^{\pi-1} \mathfrak{B}_{a,b}^1 \mathbf{P}_{a,b}(t) \\ \sum_{a=1}^m \sum_{b=0}^{\pi-1} \mathfrak{B}_{a,b}^2 \mathbf{P}_{a,b}(t) \\ \sum_{a=1}^m \sum_{b=0}^{\pi-1} \mathfrak{B}_{a,b}^3 \mathbf{P}_{a,b}(t) \end{array} \right) &= \sum_{a=1}^m \sum_{b=0}^{\pi-1} \mathfrak{B}_{a,b} \mathbf{P}_{a,b}(t) = D_t^{\epsilon(\theta)} \mathfrak{w}_\pi(t) \\ &= \left( \begin{array}{c} D_t^{\epsilon(\theta)} x_\pi(t) \\ D_t^{\epsilon(\theta)} y_\pi(t) \\ D_t^{\epsilon(\theta)} y_\pi(t) \end{array} \right), \end{aligned}$$

here we have  $\pi \in \{2^i : i = 0, 1, 2, 3, \dots\}$  and

$$\begin{aligned}
 \mathfrak{B}_{a,b} &= \langle D_t^{\epsilon(\theta)} \mathfrak{w}_\pi, \mathbf{P}_{a,b} \rangle_{\mathbf{m}} = \int_0^{\mathbf{m}} D_t^{\epsilon(\theta)} \mathfrak{w}_\pi(t) \mathbf{P}_{a,b}(t) dt, \\
 \mathfrak{B}_{a,b}^1 &= \langle D_t^{\epsilon(\theta)} x_\pi, \mathbf{P}_{a,b} \rangle_{\mathbf{m}} = \int_0^{\mathbf{m}} D_t^{\epsilon(\theta)} x_\pi(t) \mathbf{P}_{a,b}(t) dt, \\
 \mathfrak{B}_{a,b}^2 &= \langle D_t^{\epsilon(\theta)} y_\pi, \mathbf{P}_{a,b} \rangle_{\mathbf{m}} = \int_0^{\mathbf{m}} D_t^{\epsilon(\theta)} y_\pi(t) \mathbf{P}_{a,b}(t) dt, \\
 \mathfrak{B}_{a,b}^3 &= \langle D_t^{\epsilon(\theta)} z_\pi, \mathbf{P}_{a,b} \rangle_{\mathbf{m}} = \int_0^{\mathbf{m}} D_t^{\epsilon(\theta)} z_\pi(t) \mathbf{P}_{a,b}(t) dt.
 \end{aligned} \tag{6.2}$$

Therefore,

$$\begin{aligned}
 D_t^{\epsilon(\theta)} \mathfrak{w}(t) - D_t^{\epsilon(\theta)} \mathfrak{w}_\pi(t) &= \sum_{a=1}^{\mathbf{m}} \sum_{b=2^i}^{\infty} \mathfrak{B}_{a,b} \mathbf{P}_{a,b}(t), \\
 &= \left( \begin{array}{l} \sum_{a=1}^{\mathbf{m}} \sum_{b=2^i}^{\infty} \mathfrak{B}_{a,b}^1 \mathbf{P}_{a,b}(t) \\ \sum_{a=1}^{\mathbf{m}} \sum_{b=2^i}^{\infty} \mathfrak{B}_{a,b}^2 \mathbf{P}_{a,b}(t) \\ \sum_{a=1}^{\mathbf{m}} \sum_{b=2^i}^{\infty} \mathfrak{B}_{a,b}^3 \mathbf{P}_{a,b}(t) \end{array} \right), \quad i = 0, 1, 2, 3, \dots
 \end{aligned} \tag{6.3}$$

At this stage, we can first assume that state coordinates  $(x, y, z)$  all belong to  $H^1[0, \mathbf{m}]$  which is a Sobolev space. This allows the exploitation of (6.1) to propose a desired result as formulated in the following theorem:

**Theorem 1.** *Having fixed  $\epsilon(\theta)$  in  $[0, 1]$  with  $\theta \in \mathbb{R}_+$ , and considered  $(x, y, z) \in [H^1[0, \mathbf{m}]]^3$ . If for  $\pi \in \{2^i : i = 0, 1, 2, 3, \dots\}$ , the general variable order  $\epsilon(\theta)$ - operator  $D_t^{\epsilon(\theta)} \mathfrak{w}_\pi(t)$  approximates  $D_t^{\epsilon(\theta)} \mathfrak{w}(t)$  via the HWNM, then such an approximation is acceptable conditional to a tolerable upper bound defined as follows.*

$$\|D_t^{\epsilon(\theta)} \mathfrak{w}(t) - D_t^{\epsilon(\theta)} \mathfrak{w}_\pi(t)\|_2 \leq \zeta \mathfrak{J}_\pi / (\epsilon, \theta),$$

where

$$\mathfrak{J}_\pi(\epsilon, \theta) = \frac{1}{\frac{3\sqrt{2}\mathbf{m}}{2(\Gamma(1-\epsilon(\theta)))(1-\epsilon(\theta))} \left( \frac{(1-1\pi^{(1-\epsilon(\theta))})}{(\pi^{\frac{3}{2}})2^{2\epsilon(\theta)-1-1}} + \frac{(1-1\pi^{(3-2\epsilon(\theta))})}{\sqrt{\pi}2^{2\epsilon(\theta)-1}-3(\pi^{\frac{3}{2}})} \right)^{\frac{1}{2}}}, \quad \zeta \in \mathbb{R}^+.$$

*Proof.* From (6.3) and (6.1) the following equality holds

$$\begin{aligned}
 &\|D_t^{\epsilon(\theta)} \mathfrak{w}(t) - D_t^{\epsilon(\theta)} \mathfrak{w}_\pi(t)\|_2^2 \\
 &= \|D_t^{\epsilon(\theta)} x - D_t^{\epsilon(\theta)} x_\pi\|_{L^2}^2 + \|D_t^{\epsilon(\theta)} y - D_t^{\epsilon(\theta)} y_\pi\|_{L^2}^2 + \|D_t^{\epsilon(\theta)} z - D_t^{\epsilon(\theta)} z_\pi\|_{L^2}^2 \\
 &= \int_0^{\mathbf{m}} \left| \sum_{a=1}^{\mathbf{m}} \sum_{b=\pi}^{\infty} \mathfrak{B}_{a,b}^1 \mathbf{P}_{a,b}(t) \right|^2 dt + \int_0^{\mathbf{m}} \left| \sum_{a=1}^{\mathbf{m}} \sum_{b=\pi}^{\infty} \mathfrak{B}_{a,b}^2 \mathbf{P}_{a,b}(t) \right|^2 dt \\
 &\quad + \int_0^{\mathbf{m}} \left| \sum_{a=1}^{\mathbf{m}} \sum_{b=\pi}^{\infty} \mathfrak{B}_{a,b}^3 \mathbf{P}_{a,b}(t) \right|^2 dt.
 \end{aligned}$$

Making use of the Fubini-Tonelli Theorem [7, 24] and the remark that for  $0 \leq a \leq \mathbf{m}$ ,  $\{\mathbf{P}_{a,b}(t)\}_{b=0}^\infty$  is a complete orthonormal family on  $[0, \mathbf{m}]$  lead to

$$\begin{aligned} \|D_t^{\epsilon(\theta)} \mathbf{w}(t) - D_t^{\epsilon(\theta)} \mathbf{w}_\pi(t)\|_2^2 &\leq \left\{ \sum_{a=1}^{\mathbf{m}} \sum_{n=0}^\infty \sum_{b=2^n}^{2^{n+1}} \int_0^{\mathbf{m}} |\mathfrak{B}_{a,b}^1|^2 dt \right. \\ &\quad \left. + \sum_{a=1}^{\mathbf{m}} \sum_{n=0}^\infty \sum_{b=2^n}^{2^{n+1}} \int_0^{\mathbf{m}} |\mathfrak{B}_{a,b}^2|^2 dt + \sum_{a=1}^{\mathbf{m}} \sum_{n=0}^\infty \sum_{b=2^n}^{2^{n+1}} \int_0^{\mathbf{m}} |\mathfrak{B}_{a,b}^3|^2 dt \right\}, \end{aligned} \tag{6.4}$$

where we used the fact that  $\pi$  belongs to the family  $\{2^n : n = 0, 1, 2, 3, \dots\}$ , and that  $\mathfrak{B}_{a,b}^\iota$ ,  $\iota = 1, 2, 3$  is given by (6.2). Now we just have to express each  $\mathfrak{B}_{a,b}^\iota$  via (6.2) and also via (3.5) and (3.6) which define  $\mathbf{P}_{a,b}$ . Hence,

$$\begin{aligned} \mathfrak{B}_{a,b}^1 &= (2^{\frac{n}{2}+1}) \left[ \int_{\frac{\pi}{2^n}+a}^{\frac{\pi+\frac{1}{2}}{2^n}+a} D_\tau^{\epsilon(\theta)} x(\tau) d\tau - \int_{\frac{\pi+\frac{1}{2}}{2^n}+a}^{\frac{\pi+1}{2^n}+a} D_\tau^{\epsilon(\theta)} x(\tau) d\tau \right], \\ \mathfrak{B}_{a,b}^2 &= (2^{\frac{n}{2}+1}) \left[ \int_{\frac{\pi}{2^n}+a}^{\frac{\pi+\frac{1}{2}}{2^n}+a} D_\tau^{\epsilon(\theta)} y(\tau) d\tau - \int_{\frac{\pi+\frac{1}{2}}{2^n}+a}^{\frac{\pi+1}{2^n}+a} D_\tau^{\epsilon(\theta)} y(\tau) d\tau \right], \\ \mathfrak{B}_{a,b}^3 &= (2^{\frac{n}{2}+1}) \left[ \int_{\frac{\pi}{2^n}+a}^{\frac{\pi+\frac{1}{2}}{2^n}+a} D_\tau^{\epsilon(\theta)} z(\tau) d\tau - \int_{\frac{\pi+\frac{1}{2}}{2^n}+a}^{\frac{\pi+1}{2^n}+a} D_\tau^{\epsilon(\theta)} z(\tau) d\tau \right]. \end{aligned}$$

Using the Mean value theorem for definite integrals, there are two times  $\mathbf{t}_x \in \left(\frac{\pi}{2^n} + a, \frac{\pi+\frac{1}{2}}{2^n} + a\right)$  and  $\tilde{\mathbf{t}}_x \in \left(\frac{\pi+\frac{1}{2}}{2^n} + a, \frac{\pi+1}{2^n} + a\right)$  such that

$$\begin{aligned} \mathfrak{B}_{a,b}^1 &= (\sqrt{2})^n \left( \frac{1}{2^{n+1}} D_\tau^{\epsilon(\theta)} x(\mathbf{t}_x) d\tau - \frac{1}{2^{n+1}} D_\tau^{\epsilon(\theta)} x(\tilde{\mathbf{t}}_x) d\tau \right) \\ &= 2^{\left(\frac{-2-n}{2}\right)} \left( D_\tau^{\epsilon(\theta)} x(\mathbf{t}_x) d\tau - D_\tau^{\epsilon(\theta)} x(\tilde{\mathbf{t}}_x) d\tau \right). \end{aligned}$$

Using the definition of the variable order derivative (1.1) yields

$$\begin{aligned} |\mathfrak{B}_{a,b}^1| &= 2^{\left(\frac{-2-n}{2}\right)} |D_\tau^{\epsilon(\theta)} x(\mathbf{t}_x) d\tau - D_\tau^{\epsilon(\theta)} x(\tilde{\mathbf{t}}_x) d\tau| \\ &= 2^{\left(\frac{-2-n}{2}\right)} \frac{1}{\Gamma(1-\epsilon(\theta))} \left| \int_0^{\mathbf{t}_x} (\mathbf{t}_x - \xi)^{-\epsilon(\theta)} \frac{dx(\xi)}{d\xi} d\xi - \int_0^{\tilde{\mathbf{t}}_x} (\tilde{\mathbf{t}}_x - \xi)^{-\epsilon(\theta)} \frac{dx(\xi)}{d\xi} d\xi \right|. \end{aligned}$$

Since  $x \in H^1[0, \mathbf{m}]$ , there exists a real number  $\zeta_x > 0$  satisfying  $\|\dot{x}(\xi)\| \leq \zeta_x$  for all  $\xi \in (0, \mathbf{t}_x)$  and  $\xi \in (0, \tilde{\mathbf{t}}_x)$ . Therefore,

$$|\mathfrak{B}_{a,b}^1| \leq \zeta_x 2^{\left(\frac{-2-n}{2}\right)} \frac{1}{\Gamma(1-\epsilon(\theta))} \left| \int_0^{\mathbf{t}_x} (\mathbf{t}_x - \xi)^{-\epsilon(\theta)} d\xi - \int_0^{\tilde{\mathbf{t}}_x} (\tilde{\mathbf{t}}_x - \xi)^{-\epsilon(\theta)} d\xi \right|. \text{ After simplification, we obtain}$$

$$\begin{aligned} |\mathfrak{B}_{a,b}^1| &\leq \frac{\zeta_x 2^{\left(\frac{-2-n}{2}\right)}}{(1-\epsilon(\theta)) \Gamma(1-\epsilon(\theta))} |\mathbf{t}_x^{(1-\epsilon(\theta))} - (\tilde{\mathbf{t}}_x)^{(1-\epsilon(\theta))}| \\ &\leq \frac{\zeta_x 2^{\left(\frac{-2-n}{2}\right)}}{(1-\epsilon(\theta)) \Gamma(1-\epsilon(\theta))} 2^{n(1-\epsilon(\theta))}, \end{aligned} \tag{6.5}$$

knowing that  $0 < \epsilon(\theta) \leq 1$ , and where we have considered the interval of definition for  $\mathbf{t}_x$  and  $\tilde{\mathbf{t}}_x$  given above. We can repeat the same analysis to show

existence of  $\zeta_y$  and  $\zeta_z$  satisfying

$$\begin{aligned} |\mathfrak{B}_{a,b}^2| &\leq \frac{\zeta_y 2^{-\left(\frac{3}{2}+1\right)}}{(1-\epsilon(\theta))\Gamma(1-\epsilon(\theta))} 2^{n(1-\epsilon(\theta))} \\ |\mathfrak{B}_{a,b}^3| &\leq \frac{\zeta_z 2^{\left(-\frac{2-n}{2}\right)}}{(1-\epsilon(\theta))\Gamma(1-\epsilon(\theta))} 2^{n(1-\epsilon(\theta))}. \end{aligned} \tag{6.6}$$

After setting  $\zeta = \max(\zeta_x, \zeta_y, \zeta_z)$  and substituting (6.5), (6.6) into (6.4) we obtain

$$\begin{aligned} \|D_\tau^{\epsilon(\theta)} \mathbf{w}(t) - D_\tau^{\epsilon(\theta)} h_\pi(t)\|_2^2 &\leq \frac{\zeta^2}{((1-\epsilon(\theta))\Gamma(1-\epsilon(\theta)))^2} \\ &\times \left[ \sum_{a=1}^{\mathbf{m}} \sum_{n=0}^{\infty} \sum_{b=2^n}^{2^{n+1}} 2^{\left(-\frac{2-n}{2}\right)} 2^{n(1-\epsilon(\theta))} \right]^2 \leq \frac{9\mathbf{m}^2 \zeta^2}{(\Gamma(1-\epsilon(\theta)))^2 (1-\epsilon(\theta))^2} \\ &\times \left( \frac{(2-2\pi^{(1-\epsilon(\theta)))}}{(\pi^{\frac{3}{2}})2^{2\epsilon(\theta)-1}-1} + \frac{(2-2\pi^{(3-2\epsilon(\theta)))}}{\sqrt{\pi}2^{2\epsilon(\theta)-1}-3(\pi^{\frac{3}{2}})} \right) \leq \zeta^2 \left( \frac{3\sqrt{2}\mathbf{m}}{2(\Gamma(1-\epsilon(\theta)))(1-\epsilon(\theta))} \right)^2 \\ &\times \left( \frac{(1-1\pi^{(1-\epsilon(\theta)))}}{(\pi^{\frac{3}{2}})2^{2\epsilon(\theta)-1}-1} + \frac{(1-1\pi^{(3-2\epsilon(\theta)))}}{\sqrt{\pi}2^{2\epsilon(\theta)-1}-3(\pi^{\frac{3}{2}})} \right) \leq \left( \mathfrak{J}_\pi(\epsilon, \theta) \right)^2, \end{aligned}$$

and the proof is complete.  $\square$

*Remark 1.* For the states variable functions  $x, y, z \in L^2[0, \mathbf{m})$ , rather than  $H^1[0, \mathbf{m})$ , we need additional conditions to formulate the theorem as seen in the following corollary.

*Corollary 1.* Having fixed  $\epsilon(\theta)$  in  $[0, 1]$  with  $\theta \in \mathbb{R}_+$ , and considered  $(x, y, z) \in [L^2[0, \mathbf{m})]^3$ . In addition, assume that  $\frac{d}{dt}x(t)$ ,  $\frac{d}{dt}y(t)$  and  $\frac{d}{dt}z(t)$  are continuous and bounded on  $[0, \mathbf{m})$ . If for  $\pi \in \{2^i : i = 0, 1, 2, 3, \dots\}$ , the general variable order  $\epsilon(\theta)$ -operator  $D_t^{\epsilon(\theta)} \mathbf{w}_\pi(t)$  approximates  $D_t^{\epsilon(\theta)} \mathbf{w}(t)$  via the HWNM, then such an approximation is acceptable conditional to a tolerable upper bound defined as follows.

$$\|D_t^{\epsilon(\theta)} \mathbf{w}(t) - D_t^{\epsilon(\theta)} \mathbf{w}_\pi(t)\|_2 \leq \frac{\zeta}{\mathfrak{J}_\pi(\epsilon, \theta)},$$

where

$$\mathfrak{J}_\pi(\epsilon, \theta) = \frac{1}{\frac{3\sqrt{2}\mathbf{m}}{2(\Gamma(1-\epsilon(\theta)))(1-\epsilon(\theta))} \left( \frac{(1-1\pi^{(1-\epsilon(\theta)))}}{(\pi^{\frac{3}{2}})2^{2\epsilon(\theta)-1}-1} + \frac{(1-1\pi^{(3-2\epsilon(\theta)))}}{\sqrt{\pi}2^{2\epsilon(\theta)-1}-3(\pi^{\frac{3}{2}})} \right)^{\frac{1}{2}}}, \zeta \in \mathbb{R}^+.$$

*Proof.* Since the interval  $[0, \mathbf{m})$  is not closed, this additional condition is necessary to avoid the case where the states variable functions and their derivatives finds themselves unbounded on  $[0, \mathbf{m})$  or not able to attain their bounds. The rest of the proof follows the same route as the Theorem 1.  $\square$

### 7 Numerical representations and interpretations

In this section, some numerical representations of the initial value problem (3.1)–(1.5) are implemented using the scheme presented here above. The  $\chi(y)$ – and  $\varpi(z)$ – perturbation on the system (3.1) shall be showing up and this shall allow a possible interpretation. We already have established that the dynamical evolutions of the system will lead to attractors as illustrated by Figure 7. For  $\epsilon(\theta) = 1$ , maintaining the parameter values at  $\gamma_1 = 2$ ,  $\gamma_2 = 8$ ,  $r = 4$  and considering  $\gamma_3 = 1.2$ , the system (3.1)–(1.5) depicts an attractor represented in Figure 10 (a) where the following initial conditions have been considered  $\hat{x} = 0$ ,  $\hat{y} = 2$ ,  $\hat{z} = 1$  and  $\tau = 1$ ,  $\alpha = 0$ ,  $\varpi(z) = 0$ .

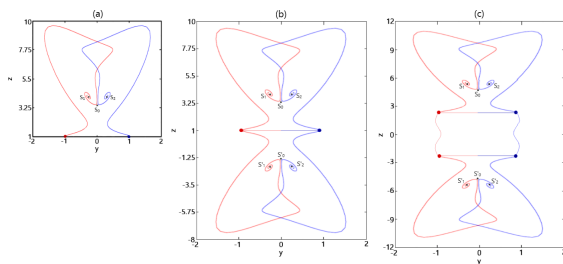


**Figure 10.** Attractor representing (3.1)–(1.5) with initial conditions  $\hat{x} = 0$ ,  $\hat{y} = 2$ ,  $\hat{z} = 1$ .

For  $\epsilon(\theta) = 0.95\theta$ ,  $\mathbf{m} = 2$ ,  $\mathbf{M} = 1$ , keeping the other parameters unchanged ( $\gamma_1 = 2$ ,  $\gamma_2 = 8$ ,  $r = 4$ ,  $\gamma_3 = 1.2$ ) with the same initial conditions,  $\hat{x} = 0$ ,  $\hat{y} = 2$ ,  $\hat{z} = 1$ , we consider now  $\tau = 3.2$ ,  $\alpha = 12$ . Taking  $\varpi(z) \neq 0$  by using  $\theta = 1.05$ ,  $\check{z} = -2.5$ ,  $z_1 = 4$  and then

$$\varpi(z) = \theta(1 + \text{sgn}(\text{sgn}(z - \check{z}) \times (z - \check{z}) - (z_1 - \check{z}))),$$

we have the mirror representation depicted in Figure 10(b) and representing a DA in a symmetrical structure facing each other with similar properties and  $z = 1$  as the symmetry line. In Figure 10(c), plotted for  $\epsilon(\theta) = 0.55\theta$  the symmetry line is moved to  $z = 0$  but the DA in a symmetrical structure is maintained.

*Remark 2. 1.* The attractor depicted in Figure 10(a) has two PAs and a total of five equilibria including one saddle node:  $(0, 0, 10/3)$  and four stable points:  $(\mp 0.6, \mp 0.3, 4)$ .

2. Due to the mirror symmetrical structure (MSS), the attractor depicted in Figure 10(b) has two pairs of PAs and a pair with five equilibria each, in the form of two saddle nodes:  $[(0, 0, 10/3); (0, 0, -4/3)]$  and the eight stable points:  $[(\mp 0.6, \mp 0.3, 4); (\mp 0.6, \mp 0.3, -2)]$ . A similar scenario holds for Figure 10(c) which has two pairs of PAs and a pair of five equilibria including:  $[(0, 0, 13/3); (0, 0, -13/3)]$  and the eight stable points:  $[(\mp 0.6, \mp 0.3, 5); (\mp 0.6, \mp 0.3, -5)]$ .

For  $\epsilon(\theta) = 1$  and maintaining the parameter values at  $\gamma_1 = 2$ ,  $\gamma_2 = 8$  and  $r = 4$  and for the value of  $\gamma_3 = 1.4$ , the system (3.1)–(1.5) depicts an attractor

represented in Figure 11(a) where the following initial conditions have been considered  $\hat{x} = 0, \hat{y} = 2, \hat{z} = 1$  and  $\tau = 1, \alpha = 0, \varpi(z) = 0$ .

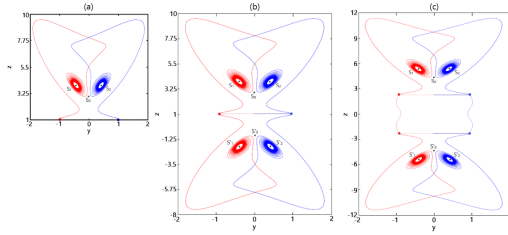


**Figure 11.** Attractor representing (3.1)–(1.5) with two limit cycles and a total of five equilibria.

Now, for  $\epsilon(\theta) = 0.95\theta, \mathbf{m} = 2, \mathbf{M} = 1$ , keeping the parameters  $\gamma_1 = 2, \gamma_2 = 8, r = 4, \gamma_3 = 1.4$  and the same initial conditions,  $\hat{x} = 0, \hat{y} = 2, \hat{z} = 1$ , we also consider  $\tau = 3.2, \alpha = 12$ . Using  $\theta = 1.05, \check{z} = -2.5, z_1 = 4$ , gives  $\varpi(z) \neq 0$  and we have the mirror representation depicted in Figure 11(b) which depicts a DA in a symmetrical structure facing each other with similar properties. The axis  $z = 1$  is its symmetry line. In Figure 11(c), plotted for  $\epsilon(\theta) = 0.55\theta$  the symmetry line is moved to  $z = 0$  but the DA in a symmetrical structure is maintained.

*Remark 3. 1.* Unlike Figure 10(a), the attractor depicted in Figure 11(a), has two limit cycles and a total of five equilibria including one saddle node:  $(0, 0, 2.8)$  and the four saddle focuses:  $(\mp 0.9, \mp 0.4, 4)$ .  
 2. Due to the MSS, the attractor depicted in Figure 11(b) has two pairs of limit cycles and a pair with five equilibria each including the two saddle nodes:  $[(0, 0, 2.8); (0, 0, -0.8)]$  and the eight stable points:  $[(\mp 0.9, \mp 0.4, 4); (\mp 0.9, \mp 0.4, -2)]$ . A similar scenario holds for Figure 11(c), which has two pairs of PAs and a pair of five equilibria that include two saddle nodes:  $[(0, 0, 3.8); (0, 0, -3.8)]$  and eight stable points:  $[(\mp 0.9, \mp 0.4, 5); (\mp 0.9, \mp 0.4, -5)]$ .

For  $\epsilon(\theta) = 1$  and maintaining the parameter values at  $\gamma_1 = 2, \gamma_2 = 8$  and  $r = 4$  and for the value of  $\gamma_3 = 2.9$ , the system (3.1)–(1.5) depicts an attractor represented in Figure 12(a), where the initial conditions have been maintained as in Figure 10(a) and  $\tau = 1, \alpha = 0, \varpi(z) = 0$ . Now, for  $\epsilon(\theta) = 0.95\theta, \mathbf{m} = 2, \mathbf{M} = 1$ , and  $\gamma_1 = 2, \gamma_2 = 8, r = 4, \gamma_3 = 2.9$  and the same initial conditions, we also consider  $\tau = 3.2, \alpha = 12$ . Using  $\varpi(z) \neq 0$  with  $\theta = 1.05, \check{z} = -2.5, z_1 = 4$ , lead to the mirror representation depicted in Figure 12(b) which depicts a DA in a symmetrical structure facing each other with similar properties. The axis  $z = 1$  is its symmetry line. In Figure 12(c), plotted for  $\epsilon(\theta) = 0.55\theta$  the symmetry line is moved to  $z = 0$  but the DA in a symmetrical structure is maintained.

*Remark 4. 1.* Unlike Figure 10(a), the representation depicted in Figure 12(a) has two SAs and a total of five equilibria including one saddle node:  $(0, 0, 1.4)$

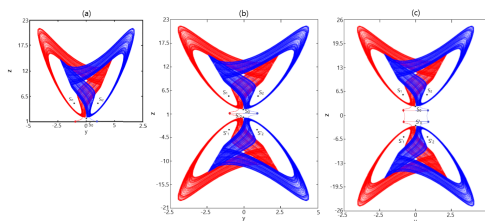


**Figure 12.** Attractor representing (3.1)–(1.5) two SAs and a total of five equilibria.

and the four saddle focuses:  $(\mp 1.9, \mp 1, 4)$ .

2. Due to the MSS, the attractor depicted in Figure 12(b) has two pairs of limit cycles and a pair with five equilibria each including the two saddle nodes:  $[(0, 0, 1.4); (0, 0, 0.6)]$  and the eight stable points:  $[(\mp 1.9, \mp 1, 4); (\mp 1.9, \mp 1, -2)]$ . A similar scenario holds for Figure 12(c), which has two pairs of PAs and a pair of five equilibria that include two saddle nodes:  $[(0, 0, 2.4); (0, 0, -2.4)]$  and eight stable points:  $[(\mp 1.9, \mp 1, 5); (\mp 1.9, \mp 1, -5)]$ .

For  $\epsilon(\theta) = 1$  and maintaining the parameter values at  $\gamma_1 = 4, \gamma_2 = 9$  and  $\gamma_3 = 4$  and for the value of  $r = 20$ , the system (3.1)–(1.5) depicts CoAs represented in Figure 13(a), where the initial conditions have been maintained as in Figure 10(a) and  $\tau = 1, \alpha = 0, \varpi(z) = 0$ . For  $\epsilon(\theta) = 0.95\theta, \mathbf{m} = 2, \mathbf{M} = 1$ , we also consider  $\tau = 3.2, \alpha = 12$ . Using  $\varpi(z) \neq 0$  with  $\theta = 1.05, \check{z} = -2.5, z_1 = 4$ , giving

$$\varpi(z) = \theta(1 + \text{sgn}(\text{sgn}(z - \check{z}) \times (z - \check{z}) - (z_1 - \check{z}))).$$

Then, we have the mirror representation depicted in Figure 13(b) which depicts two pairs of CoAs in a symmetrical structure facing each other with similar properties. The axis  $z = 5.5$  is its symmetry line. In Figure 13(c), plotted for  $\epsilon(\theta) = 0.55\theta$  the symmetry line is moved to  $z = 0$  but the structure of the two pairs of CoAs in a symmetrical representation is maintained.

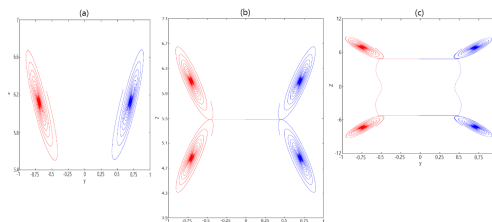


**Figure 13.** A CoAs representing (3.1)–(1.5) with  $\varpi(z) = \theta(1 + \text{sgn}(\text{sgn}(z - \check{z}) \times (z - \check{z}) - (z_1 - \check{z})))$ .

## 8 Programmed hardware implementation via FPGA development board

As the global trend in the world is becoming more and more oriented to the digital hardware circuit, many authors have opposed it to the analog hardware circuit, saying that the former provide us with a robust control and a reliable stability, two factors very important is security technologies [17,23]. Moreover, FPGA implementation has also been applied in connecting people and smart devices within the so-called Internet of things [19]. Hence, for that reason, we use a FPGA which has been reprogrammed and interconnected to meet the reliable functionality of our application. The basic principle of that flow diagram is shown in Figure 14. This gives a hardware block of the digital circuit

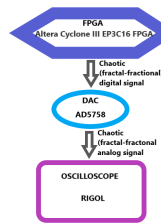


**Figure 14.** Representation of the basic principle for the implementation using the FPGA development board.

with the FPGA Developer-board with a low-power but high-performance Altera Cyclone III EP3C16 FPGA, a device offering about 15,408 Les, 56 M9K Embedded memory blocks and 504K total RAM bits. It also contains a single-channel, voltage and current output digital-to-analog converter (DAC) of series AD5758. The ultimate goal is to generate DAs or multiple attractors with their possible mirror images and perturbed mirror representations via the variable order operator. Using the DAC converter, we can therefore easily transform the digital signals into the analog signals that is directed into the RIGOL digital oscilloscope which records and keeps the resulting phase diagrams. For concerns about the level of unwanted disturbance in the signals and any alteration of their original shape, we can analyze the intermodulation distortion (IND), [12,13,22] where we consider an input signal  $\mathbb{I}_{\epsilon,\theta}(t)$  which contains only two frequency components at  $\rho_{\epsilon,\theta}^1$  and  $\rho_{\epsilon,\theta}^2$  and taking the form

$$\mathbb{I}_{\epsilon,\theta}(t) = \mathcal{A}_1 \sin(2\pi\rho_{\epsilon,\theta}^1 t + \beta_{\epsilon,\theta}^1) + \mathcal{A}_2 \sin(2\pi\rho_{\epsilon,\theta}^2 t + \beta_{\epsilon,\theta}^2)$$

with  $\mathcal{A}_i$  and  $\beta^i$  respectively representing the amplitudes and phases of each of the components. The output signal will include the original two frequencies of and also their linear combinations (LCs). Graphs (a) to (h) in Figure 15 summarize the level of such disturbance IND( $\theta$ ) for our mirror model with regard to the parameters values  $\theta = 0.3, 0.5, 0.9, 1, 1.05, 2, 2.5, 3$  respectively. As expected the results coincide with those found in the stability and entropy analysis (Sections 4 and 5).

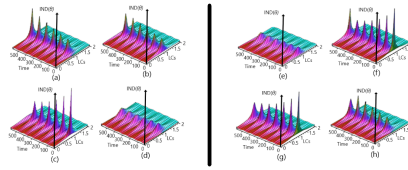


**Figure 15.** Level of unwanted signal's disturbance: (a)  $\theta = 0.3$ , (b)  $\theta = 0.5$ , (c)  $\theta = 0.9$ , and (d)  $\theta = 1$ .

First of all we start with the model (2.1) easily solvable using the Crank–Nicolson method [6] to get the discretized solution by setting for  $x, y$  and  $z$  the numerical schemes for the model by taking  $t_j = j\tau$  with  $0 \leq j \leq \mathbb{N}$ ,  $N\tau = T$ . The number  $\mathbb{N}$  represents the grid points while  $t$  is the time and  $\tau$  the step size. Hence, the discretization of first order differentiation found in (2.1) using the Crank–Nicolson approach gives

$$\begin{cases} \frac{dx(t)}{dt} = \frac{x(t_j+1)-x(t_j)}{2\tau}, \\ \frac{dy(t)}{dt} = \frac{y(t_j+1)-y(t_j)}{2\tau}, \\ \frac{dz(t)}{dt} = \frac{z(t_j+1)-z(t_j)}{2\tau}. \end{cases}$$

Substituting this system into (2.1) and considering the  $\tau = 1/100000$  and initial conditions  $(\hat{x}, \hat{y}, \hat{z}) = (0, 2, 1)$ , approximated solutions  $(x_j, y_j, z_j), j \in \mathbb{N}$  are obtained. The following step is to sent to the DAC, these solutions for time series conversion, which yields the phase orbit graphs depicted by the digital output represented by the Rigol oscilloscope as shown in Figures 16 and 17(a). We can notice that it is the same attractor done in Figure 7(b). Turning now to the system (3.8) with the general variable order  $\epsilon(\theta)$  operator, we get the initial conditions set at  $\hat{x} = 0, \hat{y} = 2, \hat{z} = 1$  and  $\tau = 1, \alpha = 0, \varpi(z) = 0, \varpi(z) \neq 0$  with  $\check{z} = -2.5, z_1 = 4$ . Repeating the same time series conversion described above using the DAC yields the phase orbit with mirroring structure as depicted in Figures 16 and 17. These representations are the hardware implementations corresponding respectively to the same attractors done in Figures 11(a), 11(b), 12(a), 12(c) and 13(b).

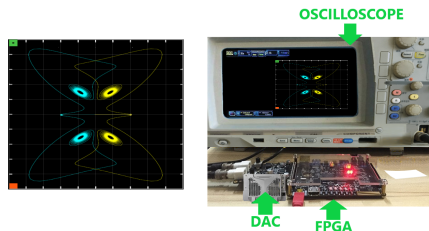


**Figure 16.** Screenshot of the system assembly and devices used during implementation with the FPGA development board.

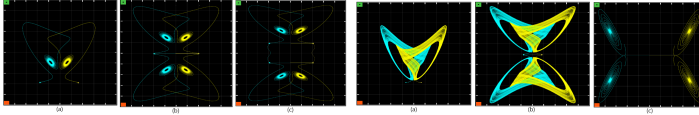


**Figure 17.** Representation of the multiple attractors before and after mirror perturbation using the FPGA implementation.

## 9 Conclusions

Based on perturbation approaches, we have inserted the duality-symmetric and the mirror symmetry conversion processes into a variable order dynamical system to finally obtain a non-linear variable order and modified initial value problem. It is represented by the electric circuit diagram with three input seen in Figure 2. We have then solved the perturbed model using the HWNM. Numerical simulations obtained from the implemented scheme have revealed existence of various attractors' types (PAs, limit cycles, SAs, DA, CoAs) and their mirror reflections. The whole picture has shown a symmetrical structure where attractors face each other with similar properties and a symmetry line between them. The circuit implementation using a Field Programmable Gate Array (FPGA) has been performed and correspond to the expected results found mathematically. These results provide us with an alternative options (either analytical or via circuit implementation) capable of creating multiple attractors with their mirror symmetrical reflections, while preserving the initial properties. Other types of non-linear perturbations and alternative circuit implementation such as digital signal processing (DSP) implementation, may be studied on similar models as doors are now open for it.

## Acknowledgements

The author likes to thank his postgraduates students for their suggestions, circuit assembly, valuable suggestions and helpful discussions.

## References

- [1] E. Babolian and A. Shahsavaran. Numerical solution of nonlinear Fredholm integral equations of the second kind using Haar wavelets. *Journal of Computational and Applied Mathematics*, **225**(1):87–95, 2009. <https://doi.org/10.1016/j.cam.2008.07.003>.
- [2] A. Banerjee, D. Singh, S. Sahana and I. Nath. Impacts of metaheuristic and swarm intelligence approach in optimization. In *Cognitive Big Data Intelligence with a Metaheuristic Approach*, pp. 71–99. Elsevier, 2022. <https://doi.org/10.1016/B978-0-323-85117-6.00008-X>.
- [3] M. Caputo. Linear models of dissipation whose  $Q$  is almost frequency independent–II. *Geophysical Journal International*, **13**(5):529–539, Reprinted in: *Fract. Calc. Appl. Anal.* 11, No 1 (2008), 3–14., 1967. <https://doi.org/10.1111/j.1365-246X.1967.tb02303.x>.

- [4] A. Chen, J. Lu, J. Lü and S. Yu. Generating hyperchaotic Lü attractor via state feedback control. *Physica A: Statistical Mechanics and its Applications*, **364**:103–110, 2006. <https://doi.org/10.1016/j.physa.2005.09.039>.
- [5] A. Chithra and I. Raja Mohamed. Multiple attractors and strange nonchaotic dynamical behavior in a periodically forced system. *Nonlinear Dynamics*, **105**(4):3615–3635, 2021. <https://doi.org/10.1007/s11071-021-06608-8>.
- [6] J. Crank and P. Nicolson. A practical method for numerical evaluation of solutions of partial differential equations of the heat-conduction type. *Advances in Computational Mathematics*, **6**(1):207–226, 1996. <https://doi.org/10.1007/BF02127704>.
- [7] G. Fubini. Opere scelte. II. *Cremonese, Roma*, 1958.
- [8] V. Gallese, P.F. Ferrari and M.A. Umiltà. The mirror matching system: A shared manifold for intersubjectivity. *Behavioral and Brain Sciences*, **25**(1):35–36, 2002. <https://doi.org/10.1017/S0140525X02370018>.
- [9] E.F. Doungmo Goufo. Stability and convergence analysis of a variable order replicator–mutator process in a moving medium. *Journal of Theoretical Biology*, **403**:178–187, 2016. <https://doi.org/10.1016/j.jtbi.2016.05.007>.
- [10] E.F. Doungmo Goufo. Strange attractor existence for non-local operators applied to four-dimensional chaotic systems with two equilibrium points. *Chaos: An Interdisciplinary Journal of Nonlinear Science*, **29**(2):023117, 2019. <https://doi.org/10.1063/1.5085440>.
- [11] E.F. Doungmo Goufo. The proto-Lorenz system in its chaotic fractional and fractal structure. *International Journal of Bifurcation and Chaos*, **30**(12), 2020. <https://doi.org/10.1142/S0218127420501801>.
- [12] K.J. Havens and E. Sharp. *Thermal imaging techniques to survey and monitor animals in the wild: a methodology*. Academic Press, 2015.
- [13] K.H. Kim and S.J. Kim. A wavelet-based method for action potential detection from extracellular neural signal recording with low signal-to-noise ratio. *IEEE Transactions on Biomedical Engineering*, **50**(8):999–1011, 2003. <https://doi.org/10.1109/TBME.2003.814523>.
- [14] Y. Li, Z. Li, M. Ma and M. Wang. Generation of grid multi-wing chaotic attractors and its application in video secure communication system. *Multimedia Tools and Applications*, **79**(39):29161–29177, 2020. <https://doi.org/10.1007/s11042-020-09448-7>.
- [15] E.N. Lorenz. Deterministic nonperiodic flow. *Journal of the Atmospheric Sciences*, **20**(2):130–141, 1963. [https://doi.org/10.1175/1520-0469\(1963\)020<0130:DNF>2.0.CO;2](https://doi.org/10.1175/1520-0469(1963)020<0130:DNF>2.0.CO;2).
- [16] J. Lü and G. Chen. Generating multiscroll chaotic attractors: theories, methods and applications. *International Journal of Bifurcation and Chaos*, **16**(04):775–858, 2006. <https://doi.org/10.1142/S0218127406015179>.
- [17] Z.T. Njitacke, L.K. Kengne et al. Antimonotonicity, chaos and multiple coexisting attractors in a simple hybrid diode-based jerk circuit. *Chaos, Solitons & Fractals*, **105**:77–91, 2017. <https://doi.org/10.1016/j.chaos.2017.10.004>.
- [18] J.S. Richman and J.R. Moorman. Physiological time-series analysis using approximate entropy and sample entropy. *American Journal of Physiology-heart and Circulatory Physiology*, **278**(6):H2039–H2049, 2000. <https://doi.org/10.1152/ajpheart.2000.278.6.H2039>.

- [19] A. Rupani and G. Sujediya. A review of FPGA implementation of internet of things. *International Journal of Innovative Research in Computer and Communication Engineering*, **4**(9):16203–16203, 2016.
- [20] M.-Z. Shieh and S.-C. Tsai. Computing the ball size of frequency permutations under Chebyshev distance. *Linear Algebra and its Applications*, **437**(1):324–332, 2012. <https://doi.org/10.1016/j.laa.2012.02.016>.
- [21] A. Simon and E.G. Boyer. *Mirrors for Behavior III. An Anthology of Observation Instruments*. 1974.
- [22] S. Temme and P. Brunet. A new method for measuring distortion using a multitone stimulus and noncoherence. *Journal of the Audio Engineering Society*, **56**(3):176–188, 2008.
- [23] E. Tlelo-Cuautle, J.D. Díaz-Muñoz, A.M. González-Zapata, R. Li W.D., León-Salas, F.V. Fernández, O. Guillén-Fernández and I. Cruz-Vega. Chaotic image encryption using hopfield and hindmarsh–rose neurons implemented on FPGA. *Sensors*, **20**(5):1326, 2020. <https://doi.org/10.3390/s20051326>.
- [24] L. Tonelli. Sull'integrazione per parti. *Rend. Acc. Naz. Lincei*, **5**(18):246–253, 1909.